Defense Technical Information Center
Compilation Part Notice

ADP014185

TITLE: Numerical Simulation of Manoeuvring Aircraft by Aerodynamic and Flight-Mechanic Coupling

DISTRIBUTION: Approved for public release, distribution unlimited
Availability: Hard copy only.

This paper is part of the following report:

TITLE: Reduction of Military Vehicle Acquisition Time and Cost through Advanced Modelling and Virtual Simulation [La reduction des couts et des delais d'acquisition des vehicules militaires par la modelisation avancee et la simulation de produit virtuel]

To order the complete compilation report, use: ADA415759

The component part is provided here to allow users access to individually authored sections of proceedings, annals, symposia, etc. However, the component should be considered within the context of the overall compilation report and not as a stand-alone technical report.

The following component part numbers comprise the compilation report:
ADP014142 thru ADP014198

Numerical Simulation of Manoeuvring Aircraft by Aerodynamic and Flight-Mechanic Coupling

A. Schütte, G. Einarsson
A. Madrane, B. Schöning
DLR
Institute of Aerodynamics and Flow Technology
Lilienthalplatz 7
D-38108 Braunschweig
Germany

W. Mönnich
DLR
Institute of Flight Research
Lilienthalplatz 7
D-38108 Braunschweig
Germany

W.-R. Krüger
DLR
Institute for Aeroelasticity
Vehicle System Dynamics
Oberpfaffenhofen
D-82234 Weßling
Germany

Summary

This paper presents results of simulations performed within the scope of the DLR-Project AeroSUM-"**Aero**dynamic **S**imulation of **U**nsteady **M**anoeuvres". The objective of the AeroSUM-Project is to develop a numerical tool to simulate the unsteady aerodynamics of a free flying aircraft, by use of coupled aerodynamic and flight-mechanic computations. To achieve this objective, the unstructured, time accurate CFD flow-solver Tau is coupled with a computational module solving the flight-mechanic equations of motion. By use of an overlapping grid technique (chimera), simulations of a complex configuration with movable control-surfaces is possible.

Results of static calculations are presented to show the basic aerodynamics of the vortex dominated flow-field of the delta wing. The static simulation cases also serve as starting solutions for the unsteady simulations. Results of the unsteady manoeuvre simulations are divided into guided motion and free-flight motion. For the guided motion an oscillating motion with a given frequency and amplitude is presented. For the free-flight motion, the following cases are presented: free-to-roll from a non-zero initial roll-angle (without flap deflection), and free-to-roll initiated by flap deflection from an initial roll-angle of zero. These calculations demonstrate the functionality of the simulation system.

A 65-degree cropped delta wing model, with fuselage and movable trailing edge flaps, is used to gather experimental data. Several forced and free-to-roll experiments around the body fixed axes, both with and without flap deflection, are performed in order to validate the computational results obtained with the simulation tool.

Nomenclature

Θ	Incidence angle, pitch angle at $\phi=0°$	Ma	Mach number
α	Angle of attack	V_∞	On flow velocity
Φ	Roll angle	$Re=V_\infty c_{ref}/\nu$	Reynolds number
$\Delta\Phi$	Roll angle amplitude	T_0	Reference temperature
η	Flap deflection angle	ν	Kinematic viscosity
y	Span-wise coordinate	$c_M=M/(q_\infty F c_{refM})$	Pitching moment coefficient
s	Half-span	$c_L=L/(q_\infty F)$	Lift coefficient
S	Reference area	$c_P=(p-p_\infty)/q_\infty$	Pressure coefficient
c_{ref}	Chord length of the model	$c_l=l/(q_\infty F c_{refl})$	Roll moment coefficient
c_{refM}	Reference length pitching moment	f	Frequency
$c_{refl}=s$	Reference length rolling moment	t	time
$c_B=0.676\,c_{ref}$	Balance reference point		

Introduction

The improvement of manoeuvrability and agility is a substantial requirement of modern fighter aircraft. Currently, roll-rates of 200°/s and more can be achieved, especially if the design of the aircraft is inherently unstable. Most of today's and probably future fighter aircraft will be delta wing configurations. The flowfield of such configurations is dominated by vortices developed by flow separation at the wings and the fuselage. The delay in time of vortex position and condition to the on-flow conditions of the manoeuvring aircraft can lead to significant phase shifts in the distribution of loads. In this case, reliable results for the analysis of flight properties can only be achieved by a non-linear integration of the unsteady aerodynamic and real flight movement. Today, these types of data can only be obtained by flight tests, and not during the design period. Flight tests, as well as modifications after the design phase, lead normally to an increase in costs. In order to decrease the costs incurred by extensive flight-tests and the post-design phase modifications, it would be helpful to have a tool which enables aircraft designers to analyse and evaluate the dynamic behaviour during the design phase.

The basic aerodynamic behaviour of a rolling delta wing is described by various authors, e.g. Er-Ei and Weihs [1], Katz and Levin [2], Gordnier[3], Gordnier and Visbal [4], as well as Ericsson [5][6]. Fore the dynamic forced and free-to-roll delta wing there exist several sources by Hanff [7] et al. [8][9][10], Hsia et al. [11], Ericsson [12] et al. [13], Chaderjian [14] and Schiff [15], Stephens [16], Jenkins [17] et al. [18], Jobe et al. [19] and Grismer et al. [20]. All these investigations were done by using structured CFD methods and only the clean delta wing without moveable control devices was considered.

To address the challenge of simulating the dynamic behaviour of fighter aircraft during a flight-manoeuvre, a simulation tool is being designed within the framework of the DLR project AeroSUM. The software package is divided into several independent modules, which can communicate with each other via a computational interface. The computational interface manages the work- and data-flow between the modules, and also serves as the main user interface. By using an unstructured CFD method in connection with an overlapping grid technique, the capability to handle highly complex configurations with components in relative motion is obtained. For the validation of the numerical results, extensive wind tunnel tests are performed, using a generic delta-wing model. **Figure 1** shows schematically the workflow management, data flow and the components of which the simulation tool consists.

1. Solution Algorithm

1.1. CFD Solver Tau

For the simulation of the flow-field around the object of interest the CFD-code Tau, developed by the DLR Institute of Aerodynamics and Flow Technology, is used [21]-[23]. The code solves the compressible, three-dimensional, time accurate Reynolds-Averaged Navier-Stokes equations using a finite volume formulation. The Tau-code is based on an unstructured-grid method. This method makes use of the advantages that hybrid grids offer in the resolution of viscous shear layers near walls, and the flexibility in grid generation offered by unstructured meshes. In order to make the flow-solver independent from the cell types in the initial grid, a dual mesh approach is used. The meshes used in the AeroSUM project are created using the hybrid mesh generator Centaur, developed by CentaurSoft [24]. The unstructured-grid approach is chosen due to its flexibility in creating grids for complex configurations, e.g. a full-configured fighter aircraft with control-surfaces and ordnance.

In the Tau-Code, a central scheme with artificial dissipation, as well as several upwind schemes, are available for spatial discretization. Both Spalart-Allmaras and k-ω turbulence models are implemented. For the results shown in this paper the Spalart-Allmaras turbulence model is used. For steady calculations an explicit multistage Runge-Kutta time stepping scheme is used. For time accurate computations, an implicit dual time stepping approach is used. The Tau-Code is parallelised using grid partitioning, and a multi-grid approach is used in order to increase the performance.

The Tau-Code consists of several different modules: the pre-processor uses the information from the initial grid to create a dual-mesh; the solver performs the flow-calculations using the approaches listed above; the adaptation module is used to refine the mesh to better capture flow phenomena like vortex structures and shear layers near viscous boundaries, among others; the post-processing module is used to create visual representations of the solver output. Furthermore, the overlapping grid technique is used to enable calculations of manoeuvre simulations with movable flaps. The chimera technique is chosen due

to its ability to handle large-amplitude deflections of the control-surfaces, the movement of the model in wind-tunnel surroundings, and the option to extend it in the future to allow for store-release simulations. The chimera mesh for the delta wing with trailing edge flaps is shown in **Figures 2** and **3**. In Figure 2 the surface mesh of the delta wing and the chimera boundaries are shown. On the right side, coloured red, is the boundary of the cut- out background model mesh, and on the left side, coloured green, the boundary of the flap mesh. In Figure 3 the overlapping area of the model and flap mesh is depicted. The flap mesh in this case is created to provide a flap deflection of ±15°. A more detailed description is given in references [25] and [26].

1.2. Tau-Code Extension: Chimera Technique

The chimera technique, as implemented in the Tau-Code, provides the capability to simulate large-amplitude control-surface deflections, as mentioned above. The technique is based on creating overlapping unstructured hybrid grids to handle a time-dependent relative motion of different geometries. The use of the overset concept for unstructured grids was first explored by Nakahashi et al. [27] to solve the Euler equations. The concept has been extended to unstructured hybrid grids for Navier-Stokes equations within the scope of the AeroSUM project.

In the overlapping grids concept, there are two major procedures involved in establishing intergrid communications. The first procedure is hole cutting (automatic or manual). For the cases presented in this paper, manual hole cutting is used. The second procedure is the identification of interpolation stencils, which involves a search of donor cells for all intergrid boundary points. The interpolation is based on the finite element theory, as presented by Ciarlet [28]. Two types of interpolation are implemented. In case the various control volume elements (prisms, hexahedrons, pyramids) are subdivided into tetrahedrons, a linear interpolation is performed. If no subdivision is used a non-linear finite element type interpolation is used. The search algorithm is based on a state-of-the-art alternating digital tree (ADT) data structure [29]. The ADT data structure optimises the search operations to O(logN/log2) as opposed to the total number (N) of elements in the computational domain.

The current implementation of the chimera technique can handle both steady and unsteady simulations for inviscid and viscous flows with multiple moving bodies. The technique currently runs in sequential mode on both workstation and supercomputer (NEC SX5) architectures.

1.3. Tau-Code Extension: Multi-Body Relative Motion

In order to utilise the capabilities offered by the chimera technique, a hierarchy for multi-body relative motion is implemented in the AeroSUM version of the Tau-Code. The current implementation can handle an arbitrary number of moving bodies, as well as an arbitrary depth of branches on the hierarchy list. The motion of each body, and the parent-node it belongs to, are specified in separate files for each body. The available motion types are conventional periodic motion for oscillation, specified with Fourier series and a reduced frequency, and rigid motion for constant rotation, specified with a polynomial series.

For coupled aerodynamic-flight-mechanic simulations, an external module handles the calculations of the motion of the control surfaces relative to the aircraft, while the aircraft motion is handled by the flight-mechanic module. The motions of the control surfaces are specified via a polynomial series, which is based off of the actual motion of the control surfaces during the wind-tunnel experiments.

1.4. Flight Mechanics

For the numerical simulation of the flight mechanics, the multi-body simulation software SIMPACK is used. SIMPACK is developed for the simulation of mechanical systems (automotive, aerospace, etc.) by the DLR Institute for Aeroelasticity in Oberpfaffenhofen. In cooperation with the DLR Institute of Flight Research, the software has been implemented with a module, which solves the flight-mechanic equations of motion. Initially, the numerical integration of the flight-mechanic equations was performed using a first-order Euler explicit scheme. Recently, a second-order Runge-Kutta scheme has been implemented to increase the performance and stability of the integration, thus allowing for increased complexity in the cases to be simulated. See also reference [30].

1.5. Computational Interface – KAPS

For the work- and data-flow management between the several modules that make up the simulation tool, for which the schematic is shown in Figure 1, a computational interface called KAPS [31] has been developed. The interface is based on a socket and thread structure, that allows the different modules to be executed on several different machines, as well as on different architectures, during a single simulation. Currently, the user interface is completely based on text-files, which are used to specify the set-up of a given simulation. In the near future, a graphical user-interface will be developed, based on the TENT [32] simulation environment, developed by DLR. Some initial results of coupled simulations performed by using the KAPS interface are presented in reference [33].

2. Experimental Data

For the validation of the numerical simulation software, various wind-tunnel experiments, designed specifically for the AeroSUM project, are performed. The experiments are done in the Transonic Wind Tunnel Göttingen (TWG). In order to perform these experiments, a wind-tunnel model has been designed and built for the AeroSUM project. The model, shown in **Figure 4**, is a generic cropped delta wing configuration, with fuselage and remote controlled moveable trailing edge flaps. Measurement equipment is installed to determine the aerodynamic forces and moments on the model, as well as the span-wise pressure distribution at two cut-plane locations, at 60% and 80% chord length. For the moveable flaps experiments, a motor is installed in front of the balance support, equipped with sensors to measure the aerodynamic forces and moments acting on the flap. The experiments contained forced and free-to-roll movements around the body-fixed longitudinal axis. For the guided motion, the model is driven by a motor connected to the sting, while for the free-to-roll experiments the motor is uncoupled. The rolling apparatus and the whole testing assembly of the TWG is shown in **Figure 5**. A variety of results are presented and discussed in [34].

3. Results

In this section, recent results obtained within the framework of the DLR Project AeroSUM, are presented. These results provide a verification of the capabilities of the simulation environment.

3.1. Steady Results

The hybrid mesh used for the steady calculations without flaps is shown in **Figure 6**. Due to the lack of an unsteady adaptation within the simulation tool, it is necessary to provide a refinement of the mesh in those areas where the vortices take place over the whole simulation range. Sources implemented within the grid generation provide a fine mesh on the upper and lower side of the wing from the tip beyond the trailing edge of the CFD model. In **Figure 7** a steady solution at $Ma = 0.5$ and $\alpha = 9°$ calculated using the mesh shown in Figure 6 is presented. The leading edge is adapted once for a better discretisation of the separating vortex sheet.

The results of the static test-cases presented in this section are a good representation of the basic aerodynamics of the delta wing model at different roll angle locations. In **Figure 8** the roll moment is shown over the roll-angle range at a Mach number of 0.5 and a pitch angle of 17.7°. At this pitch angle the roll moment for small roll angles is negative, i.e. the wing is forced to turn back into the trim point of $\phi = 0°$. At a roll angle of $\phi \approx 9°$ the sign of the roll moment changes and the wing is forced to roll in a clockwise direction. This discontinuity in the distribution is caused by a sudden movement of the point of vortex burst upon the luff side of the wing forward in leading edge direction. Finally at a roll angle of $\phi \approx 18°$ the second trim point is reached and the sign of the roll moment changes again. The region of statically unstable behaviour between the point of discontinuity and the second trim point is increased for cases with higher starting pitch angles. At lower pitch angles the delta wing is statically stable in the whole range of roll angles from $\phi = 0° - 90°$. The comparison between the experiments and the Navier-Stokes calculation shows a good fit at $\phi = 0°$ and 9°. For higher roll angles the flow field is completely unsteady, such that finding equivalent conditions is nigh to impossible, and therefore the differences are much more pronounced.

In **Figures 9** to **12** the comparison of the surface pressure between the Navier-Stokes calculation and the experimental data, corresponding to the flow-conditions listed above, is shown at a position of 60% chord length. At $\phi = 0°$ the pressure distribution of the calculation fits well with the experiments. At $\phi = 9°$ it is seen that the primary vortex is a little bit lower than in the experiments because of an over-represented secondary vortex. One reason for this behaviour in the numerical simulation is the usage of a single equation turbulence model, which leads to a higher dissipation in the boundary layer and to a stronger secondary vortex at lower angles of attack.

In **Figures 13** to **15** a static result of the model with trailing edge flaps using the overlapping grid technique is shown. The on-flow Mach number is 0.5, and the pitch angle is 9.3°. In Figure 13 the calculated surface pressure distribution is shown. In comparison to Figures 8 and 10 the effect of the flow through the flap gap is seen to lead to a low pressure area at the flap tip because of the jet trough the gap. The comparison between the calculated and the experimental pressure distribution at 60 and 80% chord length is shown in Figures 14 and 15. The calculated distribution fits well with the experiments at this low pitch angle.

3.2. Forced and Free-to-Roll Results

The results of the dynamic test-cases presented in this section highlight the current capabilities of the simulation tool. In **Figure 16** the integral lift and moment coefficients over roll angle are shown for a simulation of the oscillating delta wing. The pitch angle is constant at 17°, the frequency is 4Hz and the oscillation amplitude is $\Delta\phi = 20°$ around the body-fixed longitudinal axis. The hysteresis of the roll-moment coefficient moves in a counter-clockwise direction, which indicates that the system is highly damped dynamically. In **Figure 17** the hysteresis of the calculated and experimental roll-moment coefficient c_l, over the roll angle ϕ are compared. The hysteresis obtained from the calculation is larger than the experimental values. This indicates that the calculation predicts the system to be more damped than it is according to the experimental results. One of the reasons for this difference is that the calculation does not predict the bursting of the vortex correctly at these flight conditions, which has a major impact on the results in such a vortex dominated flowfield. One of the reasons for this may be a too low grid-resolution of the vortex structure, and affected flow phenomena, due to a lack of an unsteady adaptation being implemented in the simulation environment. Furthermore, as shown in the steady test-cases, the secondary vortex is predicted to be much stronger than in the experiment. A stronger secondary vortex results in higher lift on the luff side of the delta wing and consequently in a higher roll-moment. Furthermore, simulations that investigate the influence of the real-world experimental surroundings need to be done.

For the free-to-roll coupled flight-mechanics/aerodynamics simulations, two different geometries are used for the calculated simulations. The initial geometry is the same as for the forced-to-roll simulations, a clean delta wing without any control surfaces, while for the final geometry trailing-edge flaps are added. The simulations are restricted to a flight-mechanics model with one degree of freedom for motion, in these cases a rotation around the body-fixed longitudinal axis. In **Figures 18** and **19**, a comparison between a coupled flight-mechanics/aerodynamics calculation for the delta wing without flaps and the experimental simulation is shown. The delta wing is released from an initial roll angle of $\phi = 40°$, at a constant pitch angle of 17°, and moves into a trim point due to the effects of the aerodynamic forces. In Figure 18 it is seen that the trim points of the experiment and the calculation are vastly different. In the experiment the trim point is at $\phi \approx -18°$, which corresponds to one of the trim points observed in a static experimental test-case, depicted in Figure 8. The calculated trim point, however, is located at $\phi \approx 12°$. The gradient of ϕ versus time is also much higher for the calculated results, indicating that the calculation predicts a higher rotational velocity than is encountered in the experiment. The roll-moment coefficient over the roll angle, shown in Figure 19, exhibits a similar tendency towards higher than expected values, as previously observed in the forced-to-roll simulations. One reason for the differences between the calculated and experimental behaviour may be the lack of mechanical friction being modelled into the simulation, which results in a higher acceleration of the model after release; also, the effects of the experimental environment are not included in the simulation. Thus, together with the higher damped characteristic of the numerical system as previously mentioned, the numerical calculation predicts a totally different manoeuvre trajectory than the experiment indicates.

In **Figures 20** to **27**, the results of a free-to-roll simulation initiated by a prescribed flap deflection are shown. The delta wing is released from rest at a roll angle of $\phi = 0°$, and a constant pitch angle of 9.3°. The flaps are asymmetrically deflected using the prescribed polynomial shown in Figure 20, which induces a positive roll-moment on the aircraft and forces it to rotate around its longitudinal axis (a clockwise rotation when looking in the direction of the nose of the aircraft). In Figure 21 the roll moment is shown over the roll angle. The states of surface pressure distribution shown in Figures 22 to 27 are specifically marked in Figure 21. It is seen that the wing is accelerating up to a roll angle of $\phi=16°$. Figure 22 shows the surface pressure distribution at the initial state, where the roll moment is zero and the flaps are not deflected. Figure 23 shows the distribution at the first maximum of roll moment, where $\phi=2.2°$, and the flaps are half-way deflected at $\eta=2.5°$. At $\phi=16°$ the roll moment changes sign from positive to negative. The corresponding surface pressure distribution is depicted in Figure 24. At this point the flaps are fully deflected at $\eta=5°$. From here on the system is damped, and the corresponding surface pressure distributions are shown in Figures 24 to 26. As can be seen in these figures, the lower pressure distribution on the luff-side of the wing than on the lee-side causes a negative roll moment and decelerates the wing. At $\phi=50°$ the sign of the roll moment changes again, for which the corresponding pressure distribution is shown in Figure 26. The wing accelerates once again, but at a lower rate than previously, as can be seen by looking at the gradient of the roll moment in Figure 21. The corresponding surface pressure distribution, shown in Figure 27, also indicates a reduced rate of rotation, as the pressure difference between the luff- and lee-side is very slight. It is expected, according to experimental data, that the wing will enter a periodic rotational motion. The calculation would have to be continued to verify that the wing behaves as expected from the experiment.

4. Conclusions

In this paper a simulation tool designed for the simulation of manoeuvring aircraft with moveable control devices has been presented. The simulation tool combines time-accurate aerodynamics and flight mechanics calculations to achieve this objective. Verification of the functionality of the simulation tool has been shown by simulating a delta wing aircraft, with moveable trailing-edge flaps, during a roll manoeuvre.

The validation strategy for the simulation tool consisted of comparisons to experimental data for static, guided motion, and free-to-roll motion simulations. The comparison between the calculations and the experimental data revealed areas for improvement within the simulation tool. One of these required improvements is in the area of turbulence modelling for vortex-dominated flows. Investigations of alternative turbulence models that are currently available in the Tau-Code, but were not used for the cases presented in this paper, need to be done. Also, further investigations into grid adaptation for both steady and unsteady flow conditions need to be done in order to better predict flow phenomena in a vortex-dominated flowfield.

Another area that is currently being improved is the parallelization of the chimera technique inside the Tau-Code, which will result in a more efficient code and a reduction of the simulation time. Furthermore, unsteady adaptation for de-/refining the grid where needed is being implemented, which is expected to reduce the discrepancies owing to the non-dynamic grid-sources not fully capturing the vortex structures affecting the model.

The main objective of this paper is to focus on the necessity for developing an interactive, multidisciplinary engineering tool for predicting the unsteady critical states of complex manoeuvring aircraft. Such a simulation environment has to bring together aerodynamics, aeroelasticity and flight mechanics in a time accurate simulation tool. In order to deliver such a tool in the near future, the DLR Project SikMa-"Simulation of complex Manoeuvres" has been initiated to combine these three disciplines into one simulation environment.

5. References

[1] *Er-Ei, J.; Weihs, D.:* Nonlinear Aerodynamics of a Delta Wing in Combined Pitch and Roll. Journal of aircraft, 1989, vol. 26, no. 3, pp. 254

[2] *Katz, J.; Levin, D.:* Static Measurements of Slender Delta Wing Rolling Moment Hysteresis. Journal of aircraft, 1991, vol. 28, no. 4, pp. 282

[3] *Gordnier, R. E.:* Computation of Delta-Wing Roll Maneuvers.
     Journal of aircraft, 1995, vol. 32, no. 3, pp. 486

[4] *Gordnier, R.E.; Visbal, M.R.:* Numerical simulation of delta-wing roll
     Aerospace science and technology, 1998, vol. 2, no. 6, pp. 347

[5] *Ericsson, L.E.:* Analysis of the Effect of Sideslip on Delta Wing Roll-Trim Characteristics
     Journal of aircraft, 1997, vol. 34, no. 5, pp. 585

[6] *Ericsson, L.E.:* Effect of Angle of Attack on Roll Characteristics of 65-Degree Delta Wing
     Journal of aircraft, 1997, vol. 34, no. 4, pp. 573

[8] *Hanff, E.S.; Ericsson, L.E.:* Multiple roll attractors of a delta wing at high incidence
     AGARD FDP Symposium on vortex Flow Aerodynamics, AGARD CP 494, Oct. 1990, pp 31-1/10

[9] *Hanff, E.S.; Jenkins, S.B.:* Large-amplitude high-rate roll experiments on a delta an double delta
     wing
     AIAA 28th Aerospace Sciences Meeting, Reno, Jan 1990, AIAA-90-0224

[10] *Hanff, E.S., Huang, X.Z.:* Roll-induced cross-loads on a delta wing at high incidence
     AIAA 9th Applied Aerodynamics Conference, Baltimore, MD, September, 1991, AIAA 91-3223

[11] *Hsia, A.H.; Myatt, J.H.; Jenkins, J.E.:* Nonlinear and unsteady aerodynamics responses of a rolling
     65-degree delta wing
     AIAA Applied Aerodynamics Conference, Monterey, CA, August, 1993, AIAA 93-3682

[12] *Ericsson, L.E.:* Flow Physics of critical states for rolling delta wings
     Journal of Aircraft, Vol. 32, No. 3, May-June 1995

[13] *Ericsson, L.E.; Hanff, E.S.:* Unique high-angle roll dynamics of a sharp-edged 65-deg delta wing
     Journal of Aircraft, Vol. 31, No. 3, May-June 1994

[14] *Chaderjian, N.M.:* Navier-Stokes Prediction of Large-Amplitude Delta-Wing Roll Oscillations.
     Journal of aircraft, 1994, vol. 31, no. 6, pp. 1333

[15] *Chaderjian, N.M; Schiff, L.B.:* Numerical simulation of forced and free-to-roll delta wing motions
     Journal of Aircraft, Vol. 33, No. 1, January-February 1996

[16] *Stephens, E.J.:* Analyses of rolled delta wing flows using effective sweep and attack angles
     Journal of Aircraft, Vol. 32, No. 5, September-October 1995

[17] *Jenkins, J.E.:* Nonlinear aerodynamic characteristics of a 65 degree delta wing in rolling motion:
     Implication to testing and flight mechanics analysis (invited)
     AIAA 35th Aerospace Sciences Meeting & Exhibit, January 1997, Reno

[18] *Jenkins, J.E.; Myatt, J.H.; Hanff, E.S.:* Body axis rolling motion critical states of a 65-degree delta
     wing
     Journal of Aircraft, Vol. 33, No. 2, March-April 1996

[19] *Jobe, C.E.; Hsia, A.H.; Jenkins, J.E.; Addington, G.A.:* Critical states and flow structure on a 65 deg
     delta wing
     Journal of Aircraft, Vol. 33, No. 2, March-April 1996

[20] *Grismer, D.S.; Jenkins, J.E.:* Critical-state transients for a rolling 65-degree delta wing
     Journal of Aircraft, Vol. 34, No. 3, May-June 1997

[21] *Galle, M.:* Ein Verfahren zur numerischen Simulation kompressibler, reibungsbehafteter
     Strömungen auf hybriden Netzen
     DLR-FB 99-04 1999

[22] *Galle, M.; Gerhold, T.; Evans, J.:* Technical Documentation of the DLR Tau-Code
     DLR-IB 233-97/A43 1997

[23] *Gerhald, T.; Galle, M.; Friedrich, O.; Evans, J.:* Calculation of Complex Three-Dimensional
     Configurations employing the DLR Tau-Code
     AIAA-97-0167 1997

[24] *Centaur Soft:* http://www.centaursoft.com

[25] *Benek, J.A.; Buning, P.G.; Steger, J.L.:* A 3-D Chimera Grid Embedding Technique
     AIAA-85/1523 1985

[26] *Burggraf, U.; Kuntz, M.; Schöning, B.:*
     Implementation of the chimera method in the unstructured DLR finite volume code Tau
     Notes on Numerical Fluid Mechanics Volume 70 (eds W. Nitsche, H.-J. Heinemann, R. Hilbig)
     1999

[27] *Nakahashi,K.; Togashi,F.; Sharov, D.:* An intergrid boundary definition method for overset
     unstructured Grid
     AIAA. Vol 38, No.11, pp. 2077-2084, 2000

[28] *Ciarlet,Ph.:* The finite element method for elliptic problems
530 pp., North-Holland, Amsterdam.1978

[29] *Bonet, J., Peraire, J.:* An alternating digital tree (ADT) algorithm for 3D geometric searching and intersection problems
International Journal for Numerical Methods in Engineering, 31,1-17, 1991

[30] *SIMPAC:* Software distributed by INTEC GmbH
Münchener Straße 20 82234 Wessling, www.simpack.de

[31] *Seidler, G.:* Programmsteuerung für die multidisziplinäre Simulation des manövrierenden Flugzeugs
DGLR, AG STAB, Jahresbericht 1998

[32] *TENT:* http://www.sistec.dlr.de/tent

[33] *Schütte, A.; Einarsson, G.; Schöning, B.; Mönnich, W.:* Numerical Simulation of manoeuvring aircraft by coupling of CFD and computational flight mechanics
CEAS Conference for Multidisciplinary Aircraft Design and Optimisation, Cologne, June 2001

[34] *Psolla-Bress, H.; Haselmeyer, H.; Heddergott, A.; Höhler, G.; Holst, H.:* High-roll rate experiments on a delta wing in transonic flow
ICIASF Record, 2001, pp. 369-377

6. Figures
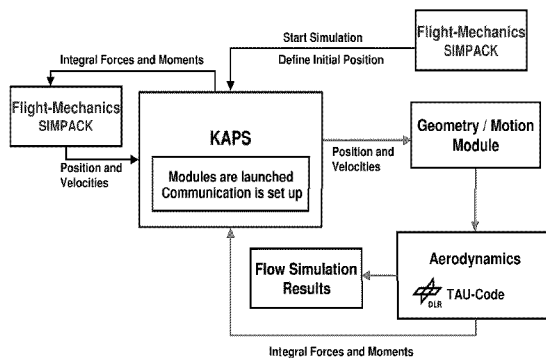
Figure 1: Work-flow and data management
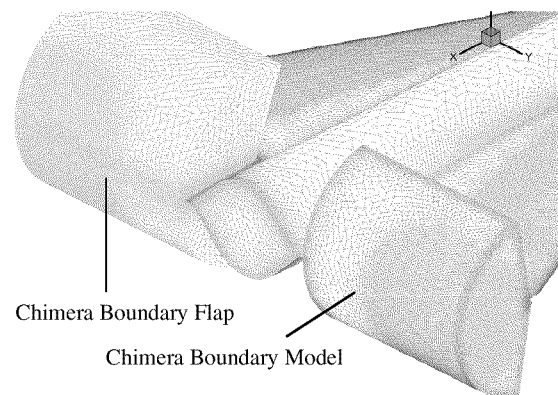
Figure 2: AeroSUM-Model: Chimera mesh
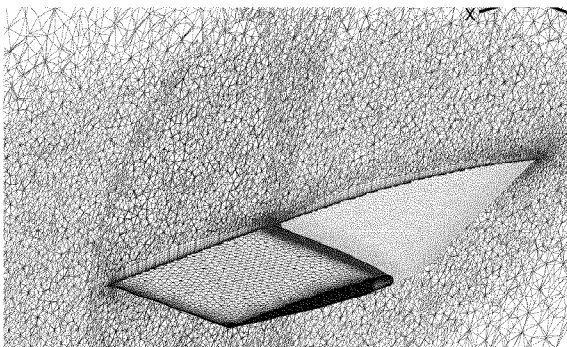
Figure 3: AeroSUM-Model:
Slice through the overlapping mesh
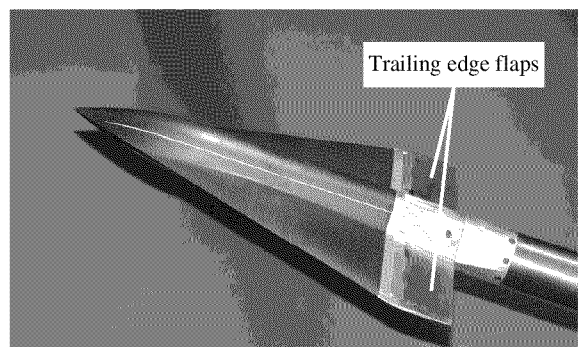
Figure 4: AeroSUM-Model
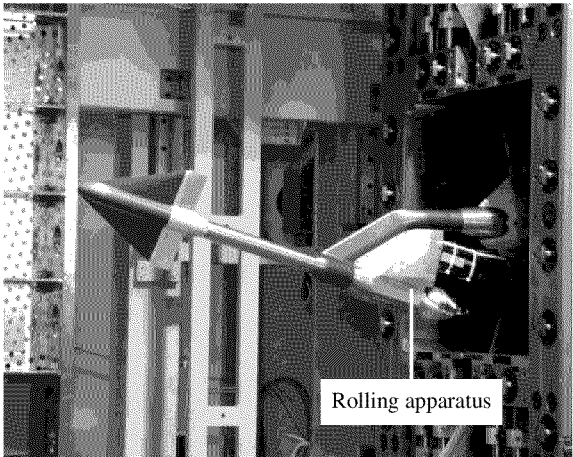
Figure 5: Test facility surrounding (TWG)
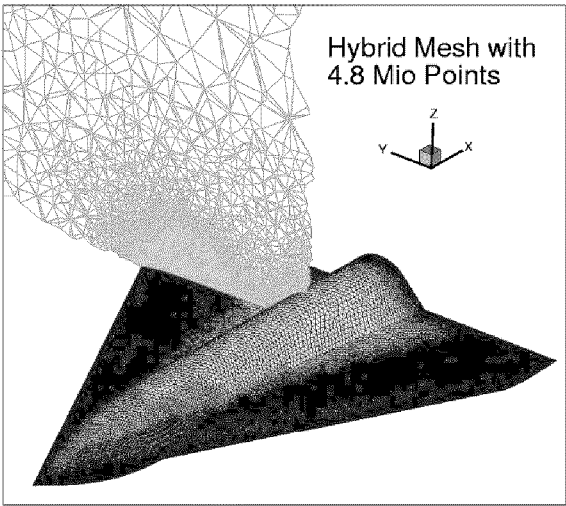
Figure 6: Unstructured Tau-Code hybrid mesh
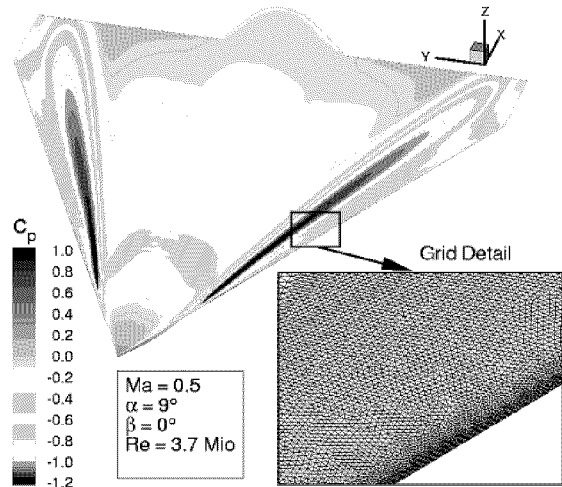
Figure 7: Tau-Code NS-Solution, adapted leading edge
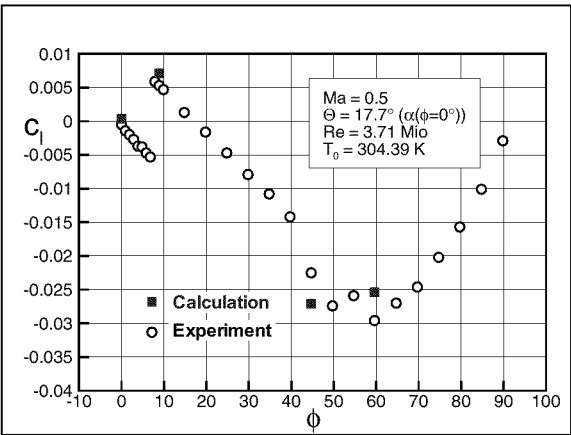
Figure 8: Integral data of a steady calculation, roll moment over roll angle
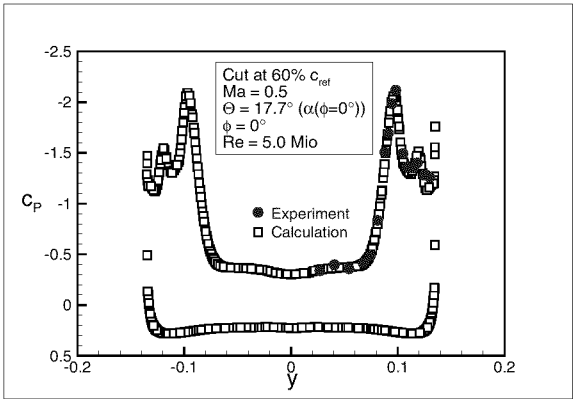
Figure 9: Pressure distribution at 60% chord length (steady case)
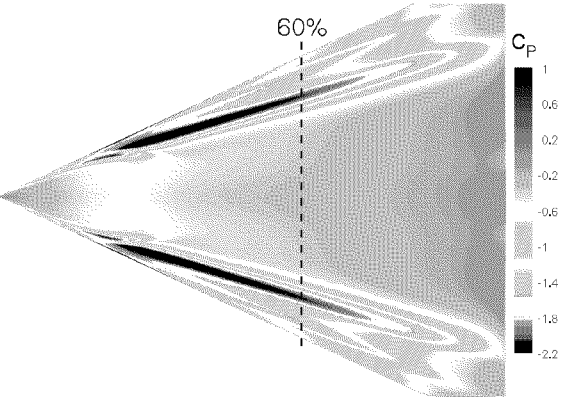
Figure 10: Surface pressure distribution, steady Navier-Stokes calculation
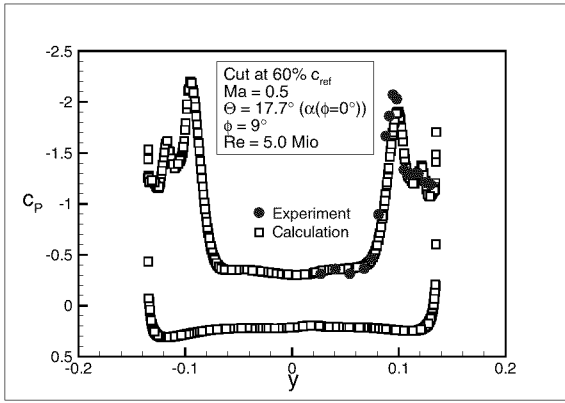
Figure 11: Pressure distribution at 60% chord length (steady case)
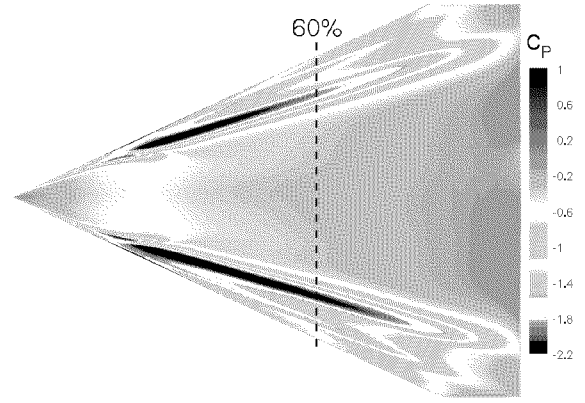
Figure 12: Surface pressure distribution, steady Navier-Stokes calculation
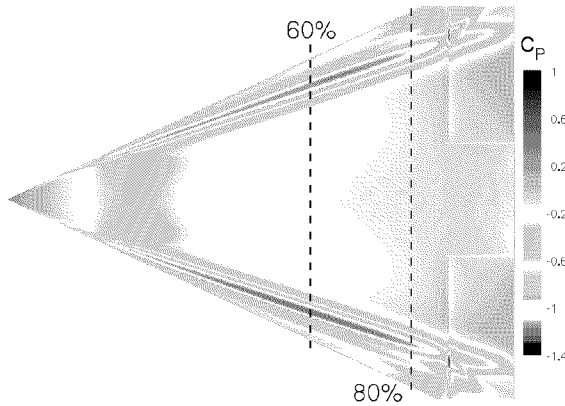
Figure 13: Surface pressure distribution, steady Navier-Stokes calculation (delta wing with flaps)
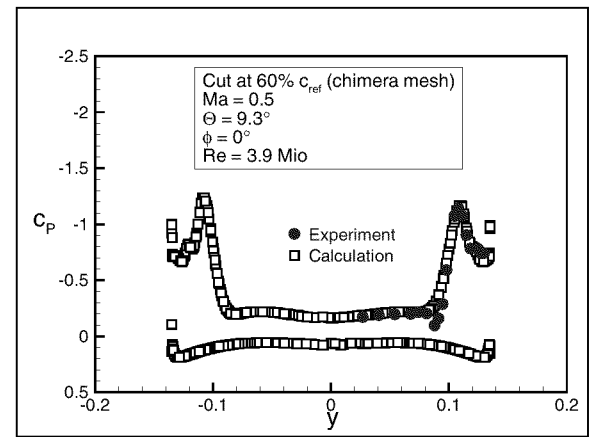
Figure 14: Pressure distribution at 60% chord length (steady case, delta wing with flaps)
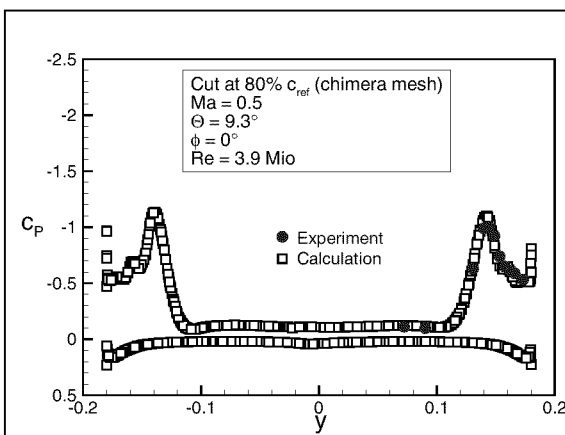
Figure 15: Pressure distribution at 80% chord length (steady case, delta wing with flaps)
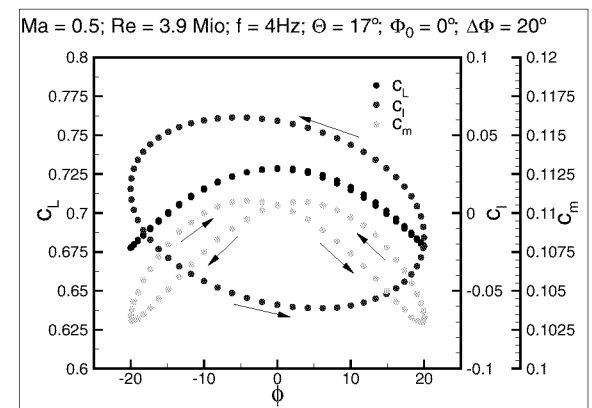
Figure 16: Integral lift, roll and pitching moment of oscillating delta wing
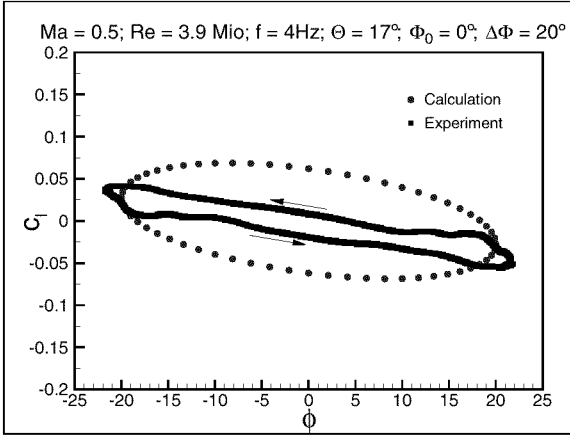
Figure 17: Comparison of experimental and calculated roll-moment for oscillating delta wing
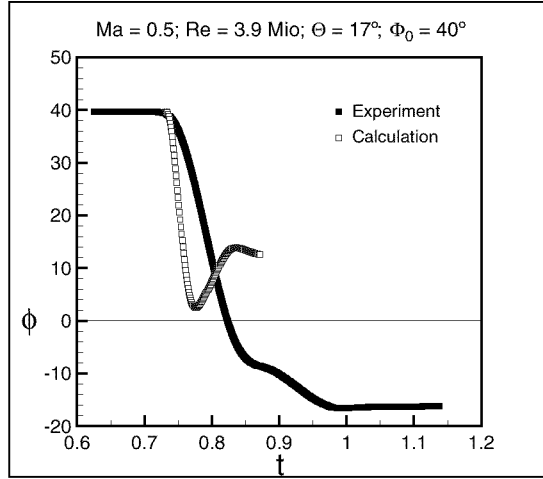
Figure 18: Roll angle ϕ over time t, free-to-roll coupled simulation
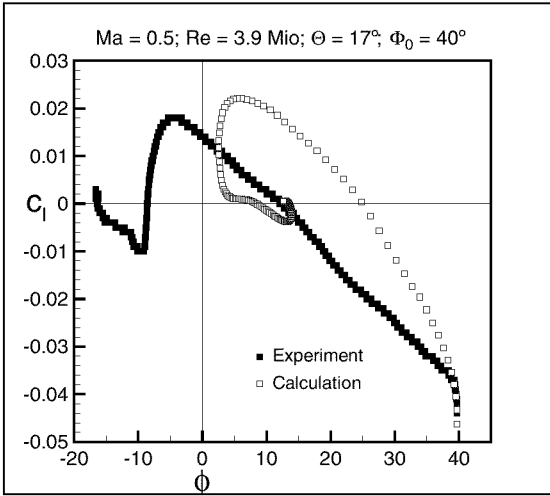
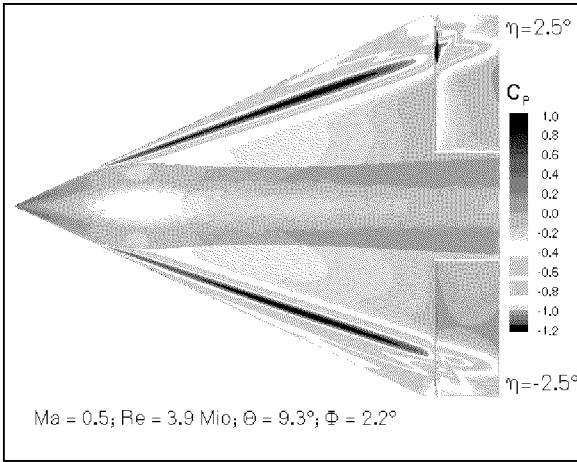Figure 19: Roll moment c_l over roll angle ϕ, free-to-roll coupled simulation
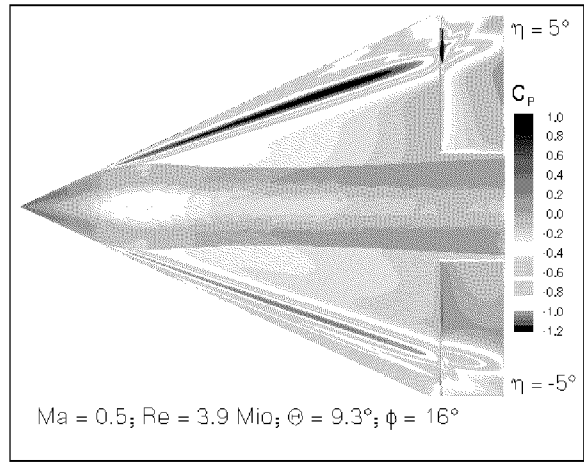

Figure 20: Flap-deflection angle over time
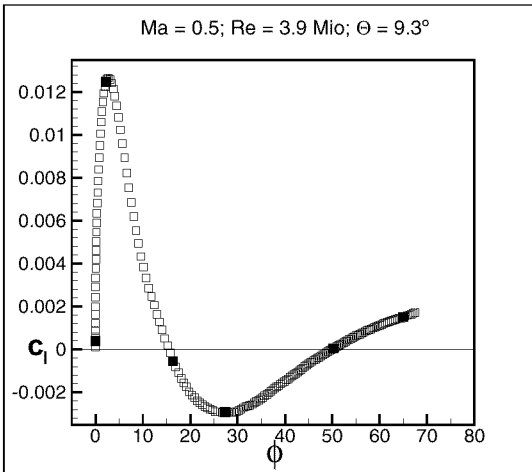
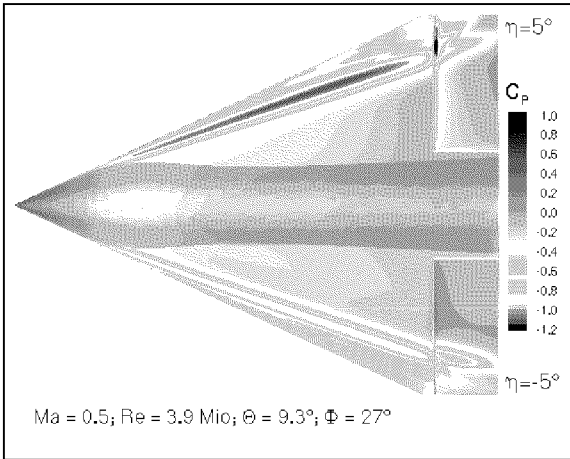Figure 21: Roll-moment over roll angle, free-to-roll coupled simulation with flap
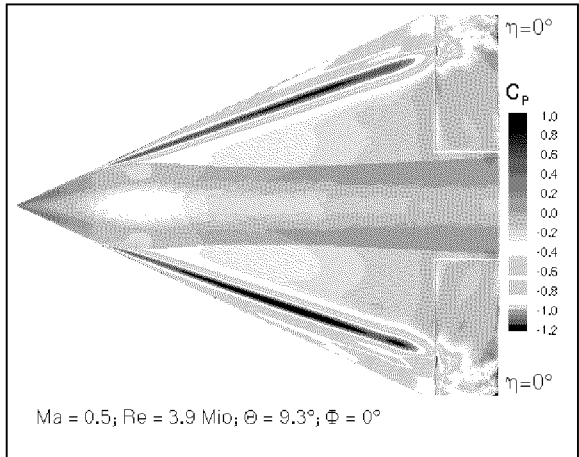
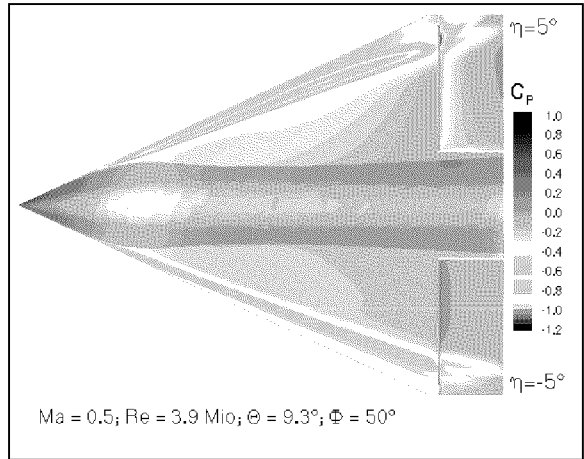Figure 22: Surface pressure distribution, free-to-roll with flap motion

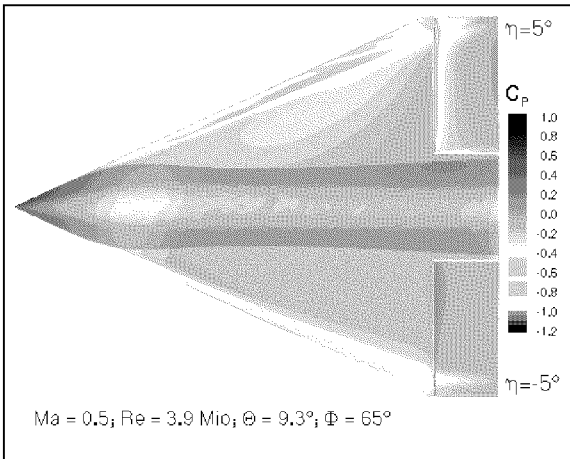**Figure 23:** Surface pressure distribution, free-to-roll with flap motion

Figure 24: Surface pressure distribution, free-to-roll with flap motion

Figure 25: Surface pressure distribution, free-to-roll with flap motion

Figure 26: Surface pressure distribution, free-to-roll with flap motion

Figure 27: Surface pressure distribution, free-to-roll with flap motion